

On the role of outer boundary condition in the collapse of molecular clouds

Motahareh Mohammadpour¹ · Maryam Ardekani¹

Received: 20 June 2016 / Accepted: 11 November 2016 / Published online: 21 November 2016
© Springer Science+Business Media Dordrecht 2016

Abstract In this paper, we investigate the influence of the outer boundary condition on the collapse of dense molecular clouds. Observational data confirm subsonic inward contraction both before and after the formation of a central protostar. Here, we study the problem of steady, spherical accretion of gas onto a protostar with the polytropic equation of state. Our model include self-gravity of the cloud and has an open outer boundary condition in which the velocity is no longer zero there. Thus, matter continuously drifts across this outer boundary. Since we study the early protostellar cloud evolution, the central protostar is highly less massive than the surrounding cloud. We assume the cloud radius is very large and impose a finite, subsonic velocity at the cloud's outer boundary and ignore magnetic field effects entirely. Our assumptions, while highly idealized, show supersonic infall is confined to the small central region of cloud.

Keywords Stars: formation

1 Introduction

Molecular clouds form the densest parts of the interstellar medium. The densest and smallest substructures of these clouds are called dense cores. Dense cores with masses about a few times the mass of the Sun and sizes of a few tenths of a parsec have been the focus of interest since they give birth to stars.

Observational studies confirm subsonic inward contraction in dense cores from asymmetric molecular emission lines (Lee et al. 2001; Goodman et al. 1998).

In dense cores with embedded low-mass stars, the inferred speeds are also subsonic in outer region. In this case, supersonic flows are confined to small central region of cloud (Choi et al. 1995; Gregersen et al. 1997; Di Francesco et al. 2001). This is not consistent with theoretical models, where the region of supersonic flow spreads outward quickly (Larson 1969; Shu 1977; Foster and Chevalier 1993; Gong and Ostriker 2009).

Stahler and Yen (2009) used perturbation theory to probe the early evolution of a spherically symmetric isothermal cloud. They concluded that this cloud underwent expanding or oscillatory motion, and would then start a long-lived subsonic accelerating collapse. Khesali et al. (2013) used the same method but relaxed the assumption of an isothermal cloud. Their model included the effects of heating and cooling rates on a spherical cloud. They found similar results as well. These studies are consistent with the observational picture (Lee and Myers 2011), that showed starless cores are static in earliest stage, and then would become expanding or oscillating in next stage and finally become contracting cores if they are sufficiently condensed.

Dense cores are parts of their parent cloud. This external environment can affect the core's evolution (Kaminski et al. 2014). A number of authors have probed the core evolution with zero inward velocity at the core's outer boundary (Larson 1969; Shu 1977; Foster and Chevalier 1993). Since there is no barrier between a dense core and its external medium, the core's boundary should be open (Mohammadpour and Stahler 2013). A number of authors investigated the modified collapse model with open boundary (Gong and Ostriker 2009, 2011; Mohammadpour and Stahler 2013; Naranjo-Romero et al. 2015). Matter can drift across this outer boundary continuously. This scheme is more realistic than the one with closed boundary.

✉ M. Mohammadpour
mohammadpour@du.ac.ir

¹ School of Physics, Damghan University, Damghan, 41167-36716, Iran

Dalba and Stahler (2012) explored how continuous, mass addition from the core’s external environment affects protostellar infall itself. They studied the collapse of a very large self-gravitating cloud with the central protostar. The cloud model was spherical and the gas temperature was isothermal. They found the mass accretion rate onto the protostar is

$$\dot{M} = 2\beta \frac{c_s^3}{G}, \tag{1}$$

where β is the Mach number of the incoming flow which is set equal to 0.2. In addition to this lowered mass accretion rate, they further showed that the region of infall spreads out at a speed near the subsonic injection velocity from the cloud’s external environment.

Real dense cores are not isothermal, but are subjected to heating and cooling processes (Goldsmith and Langer 1978; Evans et al. 2001; Crapsi et al. 2007), they can also be heated by the growing protostars. Thus, for a better understanding of collapse process, the non-isothermal cases should be included.

In this study, we prob the effect of temperature gradient on protostellar cores. For simplicity, this model is defined with a polytropic equation of state. We consider a steady state flow for a very large spherical cloud. We also impose a finite, subsonic velocity at the cloud’s outer boundary. Since we are probing the early cloud evolution, the central protostar is highly less massive than the surrounding cloud.

Although magnetic field can play an important role in collapse process, we ignore its effects entirely. This problem is like Bondi’s calculation (Bondi 1952) for spherically symmetric, polytropic flow, but include self-gravity of gas and the velocity is not zero at the outer boundary.

For this highly idealized model, gas dynamical equations and their nondimensionalization are introduced in Sect. 2. In Sect. 3, boundary conditions are presented. Section 4 gives numerical results. Finally, Sect. 5 compares these results with other studies and gives conclusions.

2 Basic equations

In this section, we derive the basic equations that govern the physics of a spherical cloud. In spherical symmetry, a steady-state continuity equation becomes

$$\frac{1}{r^2} \frac{d}{dr} (r^2 \rho u) = 0. \tag{2}$$

Under the assumption of ignoring magnetic field effects, the steady-state momentum equation becomes

$$u \frac{du}{dr} = - \frac{G(M_* + M_r)}{r^2} - \frac{1}{\rho} \frac{dP}{dr}. \tag{3}$$

Here, u is the fluid velocity, taken to be positive for inward motion and ρ is the fluid density and r is the radius of the cloud and G is the gravitational constant. The M_* and M_r are the mass of the central protostar and the cloud mass within any radius, respectively. Finally, P is internal pressure of the cloud. In this case, pressure and density are related by the polytropic equation of state

$$P = K\rho^{1+\frac{1}{n}}. \tag{4}$$

We set $\gamma = n + \frac{1}{n}$, where n is the polytropic index. Both γ and K are constants. The sound speed is introduced as follows

$$a^2 = \frac{dP}{d\rho} = \gamma K \rho^{\gamma-1}, \tag{5}$$

where a is the sound speed. Since the sound speed is dependent on local density, it is not a constant. The cloud mass M_r and radius r relation is

$$\frac{dM_r}{dr} = 4\pi r^2 \rho. \tag{6}$$

Since the flow is steady, the unchanged mass per unit time crosses every spherical shell. This constant mass accretion rate is shown by \dot{M} , where

$$\dot{M} = 4\pi r^2 \rho u. \tag{7}$$

Now, we substitute the relation $\frac{dP}{dr} = a^2 \frac{d\rho}{dr}$ into the momentum equation (3). The momentum equation becomes

$$u \frac{du}{dr} + \frac{a^2}{\rho} \frac{d\rho}{dr} + \frac{G}{r^2} (M_r + M_*) = 0. \tag{8}$$

Next, we use (2) to eliminate the density gradient in (8), the resulted equation is

$$\left(u - \frac{a^2}{u} \right) \frac{du}{dr} = \frac{2a^2}{r} - \frac{G}{r^2} (M_r + M_*). \tag{9}$$

We combine (6) and (7) into

$$\frac{dM_r}{dr} = \frac{\dot{M}}{u}. \tag{10}$$

We assume a very large cloud and set the inner and outer boundary conditions as

$$\begin{aligned} \lim_{r \rightarrow 0} u(r) &= \sqrt{\frac{2GM_*}{r}}, \\ \lim_{r \rightarrow \infty} u(r) &= u_\infty, \end{aligned} \tag{11}$$

where u_∞ is some constant, subsonic velocity at the outer boundary. Like Dalba and Stahler (2012), we suppose

$$u_\infty = \beta a_\infty, \tag{12}$$

where a_∞ is the sound speed at the outer boundary of the cloud and β is the Mach number associated with the inflow at the outer boundary. In this case, β is a constant less than one. To simplify the equations, we introduce a set of dimensional variables in terms of dimensionless ones as follow

$$\begin{aligned} u &\equiv \tilde{u}a_0, \\ a &\equiv \tilde{a}a_0, \\ r &\equiv \tilde{r}r_0, \\ \rho &\equiv \tilde{\rho}\rho_0, \\ M_r &\equiv \tilde{M}_rM_*, \\ \dot{M} &\equiv \lambda\dot{M}_0. \end{aligned} \tag{13}$$

We determine a set of fiducial quantities as

$$r_0 \equiv \frac{GM_*}{a_0^2}. \tag{14}$$

$$\rho_0 \equiv \frac{a_0^6}{G^3M_*^2}. \tag{15}$$

$$\dot{M}_0 \equiv \frac{a_0^3}{G}. \tag{16}$$

$$a_0^2 \equiv K\rho_0^{\gamma-1}. \tag{17}$$

We substitute (13) into (7), (9), (10), (11) and (12). After all tildes have been dropped, the final nondimensionalized versions of equations become

$$\frac{dM_r}{dr} = \frac{\lambda}{u}. \tag{18}$$

$$\left(u - \frac{a^2}{u}\right) \frac{du}{dr} = \frac{2a^2}{r} - \frac{(1 + M_r)}{r^2}. \tag{19}$$

$$\lambda = 4\pi r^2 \rho u. \tag{20}$$

$$a^2 = \gamma \rho^{\gamma-1}. \tag{21}$$

$$\begin{aligned} \lim_{r \rightarrow 0} u(r) &= \sqrt{\frac{2}{r}}, \\ u_\infty &= \beta a_\infty. \end{aligned} \tag{22}$$

We will alert the reader when the dimensional variables is used in Sect. 5. In order to solve (18) and (19) to obtain $u(r)$ and $M_r(r)$, we need another equation that gives $a(r)$ at any radius. Now, we combine (20) and (21) and then take the derivative of result, these equations become

$$a^2 = \gamma \left(\frac{\lambda}{4\pi}\right)^{(\gamma-1)} (r^2u)^{(1-\gamma)}, \tag{23}$$

$$\frac{da^2}{dr} = \gamma(1-\gamma) \left(\frac{\lambda}{4\pi}\right)^{(\gamma-1)} (r^2u)^{-\gamma} \left(2ru - r^2 \frac{du}{dr}\right). \tag{24}$$

The strategy is to solve (18) and (19) and (24) simultaneously to obtain $u(r)$, $M_r(r)$ and $a(r)$. For this purpose, we need to define boundary conditions and the mass accretion rate λ . In next section, we will show how we define the outer boundary conditions.

3 Boundary conditions

In previous section, we derived the basic equations that describe the physics of a spherical cloud. In this section, we need to define the boundary conditions. For our steady state flow model, u approaches a finite value for large r . Thus, $\frac{du}{dr}$ asymptotes to zero there. Then, the lefthand side of (19) goes to zero. In this way, for large r we have

$$\lim_{r \rightarrow \infty} M_r = 2r_\infty a_\infty^2 - 1. \tag{25}$$

We take the derivative of (25) as follows

$$\left(\frac{dM_r}{dr}\right)_{r \rightarrow \infty} = 2a_\infty^2 + 2r_\infty \left(\frac{da^2}{dr}\right)_{r \rightarrow \infty}. \tag{26}$$

From (23), we obtain the sound speed at large r as follows

$$a_\infty^2 = \gamma \left(\frac{\lambda}{4\pi}\right)^{(\gamma-1)} (r_\infty^2 u_\infty)^{(1-\gamma)}. \tag{27}$$

From (24), we have

$$\begin{aligned} \left(\frac{da^2}{dr}\right)_{r \rightarrow \infty} &= \gamma(1-\gamma) \left(\frac{\lambda}{4\pi}\right)^{(\gamma-1)} \\ &\times (r_\infty^2 u_\infty)^{-\gamma} (2r_\infty u_\infty). \end{aligned} \tag{28}$$

Our next task is to substitute (27) and (28) into (26). The result is as follows

$$\left(\frac{dM_r}{dr}\right)_{r \rightarrow \infty} = 2a_\infty^2(3-2\gamma). \tag{29}$$

Since the cloud mass $M_r(r)$ is an increasing function of radius, we conclude

$$2a_\infty^2(3-2\gamma) > 0, \tag{30}$$

$$\gamma < 3/2. \tag{31}$$

We find out that the values of γ must be less than 1.5. On the other hand, the lefthand side of (26) asymptotes to a finite value for large r . This clear result is obtained from (18)

$$\left(\frac{dM_r}{dr}\right)_{r \rightarrow \infty} = \frac{\lambda}{u_\infty}. \tag{32}$$

We are now able to find the fixed values of λ from (29) and (32) as follows

$$\lambda = 2a_\infty^2(3-2\gamma)u_\infty. \tag{33}$$

Table 1 Selected results of the calculations. From left to right, the columns are: γ ; density at the outer boundary; Mach number of the incoming flow; Sound speed at the outer boundary; mass accre-

tion rate; cloud outer radius; cloud total mass; sonic radius, sound speed at sonic radius and the enclosed mass within the sonic radius

γ	ρ_∞	β	a_∞	λ	r_∞	M_{r_∞}	r_s	a_s	M_{r_s}
1.00	1×10^{-9}	0.2	1.000	0.40	12615	25230	0.561	1.000	0.124
1.06	1×10^{-9}	0.2	0.553	5.95×10^{-2}	6543	3999	0.620	0.905	2.2×10^{-2}
1.08	1×10^{-9}	0.2	0.454	3.14×10^{-2}	5245	2157	0.701	0.847	1.4×10^{-2}
1.10	1×10^{-9}	0.2	0.372	1.65×10^{-2}	4199	1161	0.836	0.776	9.6×10^{-3}
1.12	1×10^{-9}	0.2	0.305	8.64×10^{-3}	3356	624	1.030	0.696	6.9×10^{-3}

For a steady state flow the values of λ are constants. If we write $\lambda = 4\pi r_\infty^2 \rho_\infty u_\infty$, then we will be able to find the density at the outer boundary as

$$\rho_\infty = \frac{(4\pi r_\infty^2)^{1/\gamma-2}}{(2\gamma(3-2\gamma))^{1/\gamma-2}}. \tag{34}$$

It is obvious from (34) that the density is a function of the cloud large radius. If we set a value for ρ_∞ and a fixed value for γ , then r_∞ can be obtained from the radius-density relation in (34). When we set ρ_∞ , we can easily find a_∞ from (21). From (22), we have $u_\infty = \beta a_\infty$. β is selected to be 0.2 (Dalba and Stahler 2012). By determining the sound speed and the flow velocity at large r , (33) then gives the value of constant λ . So far we have found $u(r)$, $a(r)$ and λ at the outer boundary. $M_r(r)$ at the outer boundary is given by

$$M_{r_\infty} = 2a_\infty^2 r_\infty - 1. \tag{35}$$

We have successfully established the outer boundary conditions. The next step is to solve (18) and (19) and (23) numerically with both the inner and outer boundary conditions. Results from the present calculations are plotted in next section.

3.1 Method of solution

Bifurcation technique (see Dalba and Stahler 2012: Sect. 2.3) is used to solve differential equations (18) and (19) and (24). This technique gives desired solutions, the ones that approach the sonic point as closely as possible and meet all the boundary conditions. The following relation, which is obtained by applying the L'Hôpital's rule to (19), gives $\frac{du}{dr}$ for each value of γ at sonic radius ($r = r_s$)

$$\left(\frac{du}{dr}\right)_{r_s} = -\frac{(2\gamma - 2)u_s^2 + \sqrt{(-6\gamma + 10)u_s^4 - \lambda(\gamma + 1)u_s}}{(\gamma + 1)r_s u_s},$$

where u_s is the flow velocity at r_s .

4 Results

In this section, we represent our numerical results. We have found the values of γ must be less than 1.5 in (31). On the other hand, the cloud with γ less than one is cooler at the center than the outer region. Since this model include the central protostar, we are interested in those values of γ which are more than one. Moreover, observational studies show that the final mass of a protostar is about 0.3 times its parent dense core (Alves et al. 2007). Since we study the early protostellar cloud evolution, the central protostar should be highly less massive than the surrounding cloud. Here, we have chosen four values of $\gamma = 1.06, 1.08, 1.10, 1.12$. We also plot $\gamma = 1.00$, for comparison with the work of Dalba and Stahler (2012).

Before starting the calculations, λ should be defined for each value of γ . For this purpose, we set $\rho_\infty = 1 \times 10^{-9}$. Then, a_∞ , u_∞ and r_∞ can be found from the relations (21), (22) and (34), respectively. The value of λ and M_{r_∞} are defined by the relations (33) and (35). Table 1 lists all the values, with the leftmost column giving the values of γ . In all these cases, the central protostars are highly less massive than the surrounding clouds.

For our selected ρ_∞ , the fourth and fifth columns in Table 1 show that a_∞ and as a result λ decrease for higher values of γ , which can be explained by relations (21) and (33). The values of r_∞ and M_{r_∞} , the sixth and seventh columns, decrease for higher values of γ as well. These results can be interpreted by the relations (34) and (35), respectively.

Figure 1 displays the non-dimensional density as a function of r for five different values of γ . The cloud with higher values of γ has less mass and mass accretion rate than the lower ones. Thus, the cloud with higher values of γ is less dense than the lower ones. Besides, the cloud undergoes gravitational collapse, and as a result, the density totally increases from the edge to the center of the cloud. From the relation (34), density is proportional to r^{-2} , $r^{-2.13}$, $r^{-2.17}$, $r^{-2.22}$, $r^{-2.27}$ at large r for $\gamma = 1.00, 1.06, 1.08, 1.10, 1.12$, respectively. The sound speed at any radius is dependent on the value of γ and the local density.

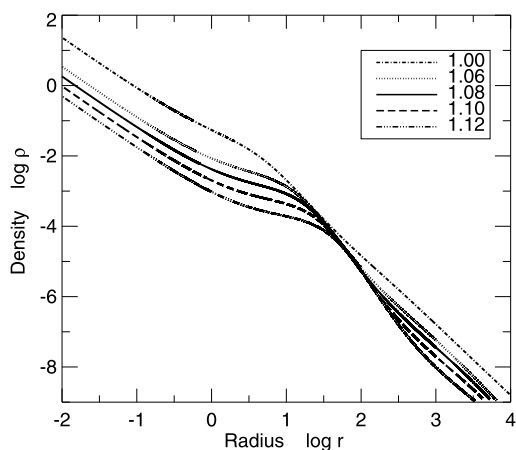


Fig. 1 Density profiles as a function of r , for the representative case $\beta = 0.2$ and $\rho_\infty = 1 \times 10^{-9}$. The lines represent $\gamma = 1.00$, $\gamma = 1.06$, $\gamma = 1.08$, $\gamma = 1.1$ and $\gamma = 1.12$

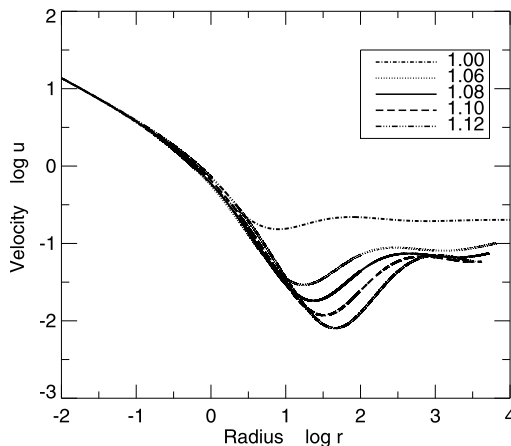


Fig. 3 Profile of velocity as a function of r , for the representative case $\beta = 0.2$ and $\rho_\infty = 1 \times 10^{-9}$. The lines represent $\gamma = 1.00$, $\gamma = 1.06$, $\gamma = 1.08$, $\gamma = 1.1$ and $\gamma = 1.12$

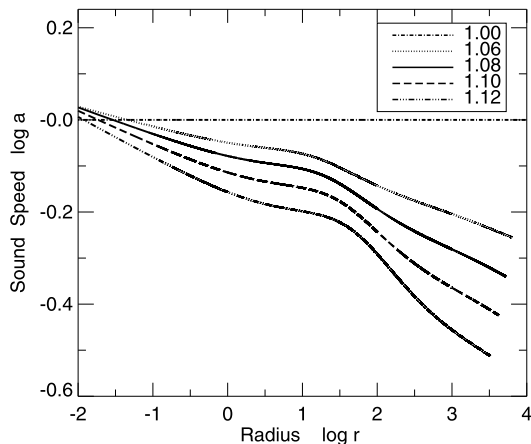


Fig. 2 Profile of sound speed as a function of r , for the representative case $\beta = 0.2$ and $\rho_\infty = 1 \times 10^{-9}$. The lines represent $\gamma = 1.00$, $\gamma = 1.06$, $\gamma = 1.08$, $\gamma = 1.1$ and $\gamma = 1.12$

Figure 2 shows that the sound speed totally increases from the outer boundary to its center for the same reason. The variation of sound speed for lower values of γ is less than the higher ones, since lower values of γ are closer to the isothermal case. Like Dalba and Stahler (2012), the sound speed remains fixed for $\gamma = 1.00$. In all cases, internal pressure totally increases inward.

Figure 3 displays the velocity profile as a function of cloud radius r . This figure shows that the flow is speeding up as it falls downward, for different values of γ , in the inner regions of cloud. Since the protostar gravity becomes dominant when reaching the center, the flow is accelerating downwards and is in a state of free-fall in the inner region of cloud. $u(r)$ asymptotically approaches βa_∞ at large r , in agreement with the imposed outer boundary condition. Thus, the gas has to make a sonic transition somewhere in between. The eighth column in Table 1 gives the values of

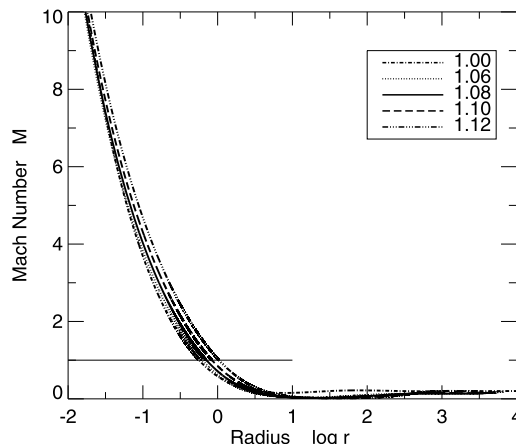


Fig. 4 Profile of Mach number as a function of r , for the representative case $\beta = 0.2$ and $\rho_\infty = 1 \times 10^{-9}$. The lines represent $\gamma = 1.00$, $\gamma = 1.06$, $\gamma = 1.08$, $\gamma = 1.1$ and $\gamma = 1.12$. The Horizontal line shows the location of sonic radius

sonic radius, r_s , for each value of γ . The ninth and tenth columns in Table 1 give the values of sound speed at sonic radius and enclosed mass within the sonic radius, respectively. r_s increases for higher values of γ . This can be understood from (19). Since at sonic radius ($u_s = a_s$), the lefthand side of (19) goes to zero, the righthand side of this equation must be zero for a smooth transition. This results in

$$r_s = \frac{(1 + M_{r_s})}{2a_s^2} \approx \frac{1}{2a_s^2}, \tag{36}$$

which shows that r_s increases as a_s decreases for higher values of γ .

Figure 4 displays Mach number ($M = u(r)/a(r)$) at all radii. The inferred flow speeds for all values of γ are subsonic in the outer region of the cloud, but supersonic within the interior. The Horizontal line in this figure shows the loca-

Table 2 Selected results of the calculations for the representative case $\gamma = 1.1$. From left to right, the columns are: γ ; density at the outer boundary; Mach number of the incoming flow; Sound speed at the

outer boundary; mass accretion rate; cloud outer radius; cloud total mass; sonic radius and sound speed at sonic radius

γ	ρ_∞	β	a_∞	λ	r_∞	M_{r_∞}	r_s	a_s
1.10	1×10^{-9}	0.2	0.372	1.65×10^{-2}	4199	1161	0.836	0.776
1.10	6×10^{-10}	0.2	0.363	1.53×10^{-2}	5284	1389	0.841	0.773
1.10	2×10^{-10}	0.2	0.343	1.30×10^{-2}	8663	2041	0.857	0.765

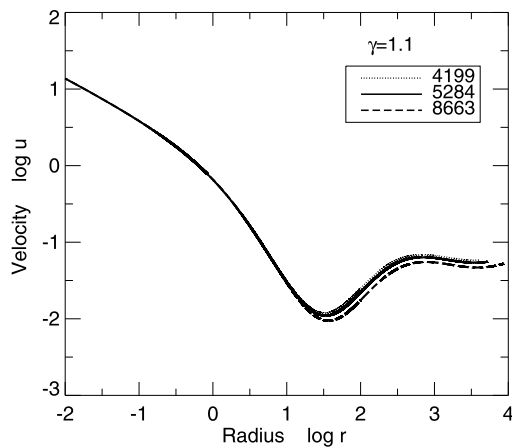


Fig. 5 Profile of velocity as a function of r , for the representative case $\beta = 0.2$ and $\gamma = 1.1$. The dotted, solid and dashed lines represent $r_\infty = 4199$, $r_\infty = 5284$ and $r_\infty = 8663$, respectively

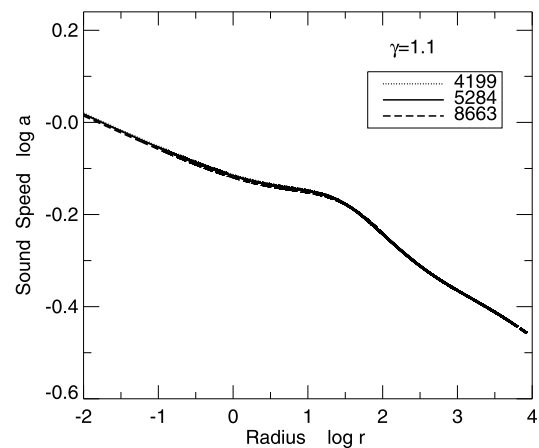


Fig. 6 Profile of sound speed as a function of r , for the representative case $\beta = 0.2$ and $\gamma = 1.1$. The dotted, solid and dashed lines represent $r_\infty = 4199$, $r_\infty = 5284$ and $r_\infty = 8663$, respectively

tion of sonic radius, where Mach number equals to one. The locations of the sonic radius are close to the central protostar for all cases, i.e. the spatial extent of supersonic infall is limited, in agreement with observational studies (Choi et al. 1995; Gregersen et al. 1997; Di Francesco et al. 2001).

In Table 2, we change the values of ρ_∞ for the representative case $\gamma = 1.1$. As the result, the outer radius and total mass of the cloud change for the different values of ρ_∞ ; however, the profiles of $\rho(r)$, $u(r)$, $a(r)$ and Mach number behave similarly to those with $\rho_\infty = 10^{-9}$. In all three cases, the surrounding cloud is highly more massive than the central protostar. These results are presented in Figs. 5, 6 and 7. It is obvious from these figures that the results are insensitive to the values of r_∞ .

5 Discussion

In this paper, we have studied the steady-state collapse model of a very large polytropic spherical cloud with the central protostar. An open outer boundary is included in this model, where matter continuously drifts across this outer boundary. Since dense cores evolve quasi-statically during a long period of slow contraction, the assumption of steady-state flow can be reasonable. Since we have probed the early

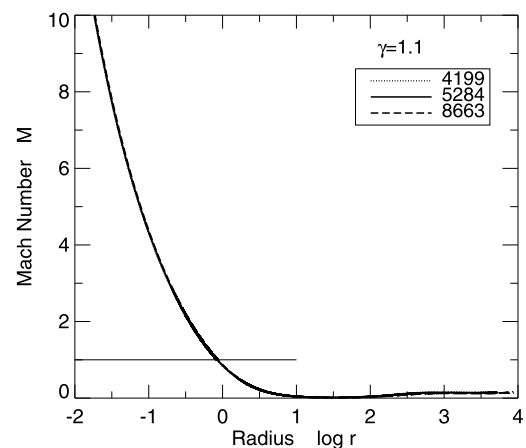


Fig. 7 Profile of Mach number as a function of r , for the representative case $\beta = 0.2$ and $\gamma = 1.1$. The dotted, solid and dashed lines represent $r_\infty = 4199$, $r_\infty = 5284$ and $r_\infty = 8663$, respectively

cloud evolution, the central protostar is highly less massive than the surrounding cloud.

It is obvious from (34) that $\rho \propto r^{-2/(2-\gamma)}$ at large r , which resembles a singular polytropic sphere “SPS” density profile (McKee and Holliman 1999; Lou and Gao 2006) in which a spherical and self-gravitating cloud is in hydrostatic

balance. Thus, the solution of this paper appears to be applicable to low-mass clouds. Besides, since the outer regions of our model cloud are nearly in hydrostatic balance, the steady state flow is an acceptable assumption. But, we need to justify this assumption for the inner supersonic infall region. For this purpose, we need

$$\frac{t_{sc}}{t_{acc}} < 1, \tag{37}$$

where t_{sc} is the dimensional sound crossing time and t_{acc} is the dimensional mass accretion timescale. We rewrite (37) in dimensional form as

$$\frac{r_s}{a_s} \frac{\dot{M}}{M_*} < 1. \tag{38}$$

Now, we use (13), (14) and (16) to write the nondimensional form of (38) as

$$\frac{r_s}{a_s} \lambda < 1. \tag{39}$$

We substitute (22), (33) and (36) into (39). Then, we have

$$\beta \left(\frac{a_\infty}{a_s} \right)^3 (3 - 2\gamma) < 1, \tag{40}$$

where $\beta < 1$, $\left(\frac{a_\infty}{a_s}\right) < 1$ and $(3 - 2\gamma) < 1$ for $\gamma > 1$, imply that t_{sc} is indeed less than t_{acc} .

The cloud model of Dalba and Stahler (2012) was isothermal, thus the flow speeding up as it falls downward and the sound speed remained constant in their model. As the result, flow velocity approached free fall onto the star and was subsonic at large distances from the star and made a sonic transition in between. Dalba and Stahler (2012) found the sonic point at 0.544 (the nondimensional radius), where Bondi’s calculation (Bondi 1952) found the sonic point at 0.5 for spherically symmetric, isothermal accretion. In contrast with isothermal case, Bondi’s calculation (Bondi 1952) found no sonic transition point for $\gamma \leq 5/3$ for spherically symmetric, polytropic accretion. The reason was that the pressure gradient which directed outward retarded the flow enough to keep it subsonic everywhere.

In this study, the values of the sonic radius are listed in Table 1 for different values of γ . In all cases, the more parts of such a cloud contain subsonic flow and the supersonic infall is confined to the small central region. This finding is in agreement with observational studies (Choi et al. 1995; Gregersen et al. 1997; Di Francesco et al. 2001).

In order to show that the sonic radius is insensitive to β , we combine (20) and (21) to write

$$\frac{a_\infty^2}{a_s^2} = \frac{\left(\frac{\lambda}{4\pi r_\infty^2 u_\infty}\right)^{(\gamma-1)}}{\left(\frac{\lambda}{4\pi r_s^2 u_s}\right)^{(\gamma-1)}}. \tag{41}$$

We substitute $u_\infty = \beta a_\infty$ and $u_s = a_s$ into relation (37). This relation becomes

$$\left(\frac{r_s}{r_\infty}\right) = \sqrt{\beta} \left(\frac{a_\infty}{a_s}\right)^{\frac{(\gamma+1)}{2(\gamma-1)}}, \tag{42}$$

where $a_\infty/a_s < 1$ and $(\gamma + 1)/2(\gamma - 1) > 1$, for $\gamma > 1$, imply that $r_s \ll r_\infty$. Note that the values of $\sqrt{\beta}$ is also less than 1, rising only from 0.45 for $\beta = 0.2$ to 0.63 for $\beta = 0.4$. Thus, we conclude that the sonic radius is insensitive to β .

For a better understanding of this problem, an account for the magnetic field and thermal effects should be included or a time-dependent calculation may solve this problem. Besides, the outer boundary in this cloud model is located, unrealistically, at infinity and a subsonic velocity is imposed there. Relaxing both these assumptions may give us a better understanding of the problem.

Acknowledgements We would like to thank the anonymous referee for providing us with constructive comments.

References

Alves, J.F., Lombardi, M., Lada, C.J.: *Astron. Astrophys.* **462**, L17 (2007)

Bondi, H.: *Mon. Not. R. Astron. Soc.* **112**, 195 (1952)

Crapsi, A., Caselli, P., Walmsley, M.C., Tafalla, M.: *Astron. Astrophys.* **470**, 221 (2007)

Choi, M., Evans, N.J., Gregersen, E.W., Wang, Y.: *Astrophys. J.* **448**, 742 (1995)

Dalba, P.A., Stahler, S.W.: *Mon. Not. R. Astron. Soc.* **425**, 1591 (2012)

Di Francesco, J., Myers, P.C., Wilner, D.J., Ohashi, N., Mardones, D.: *Astrophys. J.* **562**, 770 (2001)

Evans, N.J. II, Rawlings, J.M.C., Shirley, Y.L., Mundy, L.G.: *Astrophys. J.* **557**, 193 (2001)

Foster, P.N., Chevalier, R.A.: *Astrophys. J.* **416**, 30 (1993)

Goldsmith, P.F., Langer, W.D.: *Astrophys. J.* **222**, 881 (1978)

Gong, H., Ostriker, E.C.: *Astrophys. J.* **699**, 230 (2009)

Gong, H., Ostriker, E.C.: *Astrophys. J.* **729**, 120 (2011)

Goodman, A.A., Barranco, J.A., Wilner, D.J., Heyer, M.H.: *Astrophys. J.* **504**, 22 (1998)

Gregersen, E.M., Evans, N.J., Zhou, S., Choi, M.: *Astrophys. J.* **484**, 256 (1997)

Kaminski, E., Frank, A., Carroll, J., Myers, P.: *Astrophys. J.* **790**, 70 (2014)

Khesali, A., Nejad-Asghar, M., Mohammadpour, M.: *Mon. Not. R. Astron. Soc.* **430**, 961 (2013)

Larson, R.B.: *Mon. Not. R. Astron. Soc.* **145**, 271 (1969)

Lee, C.W., Myers, P.C.: *Astrophys. J.* **734**, 60 (2011)

Lee, C.W., Myers, P.C., Tafalla, M.: *Astrophys. J. Suppl. Ser.* **136**, 703 (2001)

Lou, Y.-Q., Gao, Y.: *Mon. Not. R. Astron. Soc.* **373**, 1610 (2006)

McKee, C.F., Holliman, J.H. II: *Astrophys. J.* **522**, 313 (1999)

Mohammadpour, M., Stahler, S.W.: *Mon. Not. R. Astron. Soc.* **443**, 3389 (2013)

Naranjo-Romero, R., Vázquez-Semadeni, E., Loughnane, R.M.: *Astrophys. J.* **418**, 48 (2015)

Shu, F.H.: *Astrophys. J.* **214**, 488 (1977)

Stahler, S.W., Yen, J.J.: *Mon. Not. R. Astron. Soc.* **396**, 579 (2009)